5-1-2010

A Study of the Dynamic Behavior of a Solid Grade SW Brick using the Split Hopkinson Pressure Bar

Erin Marie Williams

A STUDY OF THE DYNAMIC BEHAVIOR OF A SOLID GRADE SW BRICK USING THE SPLIT HOPKINSON PRESSURE BAR

By

Erin Marie Williams

A Thesis
Submitted to the Faculty of
Mississippi State University
in Partial Fulfillment of the Requirements
for the Degree of Master of Science
in Civil Engineering
in the Department of Civil and Environmental Engineering

Mississippi State, Mississippi

May 1, 2010

A STUDY OF THE DYNAMIC BEHAVIOR OF A SOLID GRADE SW BRICK

USING THE SPLIT HOPKINSON PRESSURE BAR

By

Erin Marie Williams

Approved:

Philip M. Gullett Assistant Professor of Civil and Environmental Engineering (Major Professor)	Thomas E. Lacy Jr. Associate Professor of Aerospace Engineering (Committee Member)
James D. Cargile Adjunct Professor of Civil and Environmental Engineering (Committee Member)	James L. Martin Professor and Kelly-Gene Cook, Sr. Chair in Civil and Environmental Engineering Director of Graduate Studies in the Department of Civil and Environmental Engineering
Sarah A. Rajala Dean of the James Worth Bagley College of Engineering	

Name: Erin Marie Williams

Date of Degree: May 1, 2010

Institution: Mississippi State University

Major Field: Civil and Environmental Engineering

Major Professor: Philip M. Gullett

Title of Study: A STUDY OF THE DYNAMIC BEHAVIOR OF A SOLID GRADE SW BRICK USING THE SPLIT HOPKINSON PRESSURE BAR

Pages in Study: 46

Candidate for Degree of Master of Science

The purpose of this investigation was to provide quality dynamic strength properties for a solid grade severe-weather (SW) brick material and to illustrate the need for careful evaluation of the strain-rate effects on geomaterials. A split Hopkinson pressure bar (SHPB) was used to perform a series of tests on specimens from a solid grade SW brick to determine the mechanical response of this material at high strain-rates. Both classical and modified SHPB tests were performed. The results from the classical SHPB tests provided evidence that modifications to the SHPB are necessary when testing geomaterials such as brick. To modify the SHPB, a small copper disk was placed at the impact end of the SHPB incident bar to increase the rise time of the initial pulse. The material response from the modified SHPB tests provided an average compressive strength of 104 MPa, which resulted in a dynamic increase factor of 1.42.

Key Words: split Hopkinson pressure bar, strain-rates, pulse shaping, brick

ACKNOWLEDGEMENTS

This author expresses her sincere gratitude to the people that assisted and encouraged the completion of this thesis. First of all, sincere thanks are due to Dr. Philip M. Gullett, my committee chairman, for his perseverance through the thesis process. Expressed appreciation is also due to the other members of my thesis committee, namely, Dr. Thomas E. Lacy Jr. and Dr. James D. Cargile. I also want to thank my co-workers Ed Jackson and Dr. Stephen Akers, who assisted in proofing this work. Finally, I would like to thank my family for all of their encouragement and support.

TABLE OF CONTENTS

LIST OF TABLES

LIST OF FIGURES

CHAPTER I

INTRODUCTION AND BACKGROUND

Introduction

Most material property data are obtained from results of quasi-static mechanical property tests with strain-rates on the order of 10^{-4} to 10^{-5} s^{-1}. Quasi-static mechanical property data are generally not representative of material behavior at high strain-rates. Engineers and scientists are interested in the behavior of materials when exposed to dynamic events such as high-velocity impacts and explosive detonations. Their interests are for the purposes of structural design, e.g., improving the buildings in case of earthquakes or from the blast wave of a bomb, and for developing constitutive models for numerical simulations of such dynamic events. The most common device for testing materials at high strain-rates and for characterizing the dynamic strength properties and the strain-rate effects of materials is the split Hopkinson pressure bar (SHPB). The SHPB uses one-dimensional wave propagation in elastic bars to generate a state of uniaxial stress in a specimen. The classical wave equation in terms of displacement, u, is

$$\frac{\partial^2 \mathrm{u}}{\partial t^2} = c^2 \frac{\partial^2 u}{\partial x^2} \tag{1}$$

Where t is time, x is the axial spatial position, and c is the elastic wave velocity is

$$c = \sqrt{\frac{E}{\rho}} \tag{2}$$

and E is Young's modulus while ρ is density. Equation 1 is used to derive equations that determine the stresses and strains in the test specimen. The basic concept of the SHPB is that a nondispersive elastic-stress pulse propagates through a long bar referred to as incident bar with a specimen located at the end opposite from where the stress pulse was initiated. At the incident bar-specimen interface, a portion of the stress pulse passes through the specimen into another bar referred to as the transmission bar while an elastic tensile wave (Graff, 1975) is reflected back into the incident bar. Figure 1 shows a basic SHPB test setup in which the incident and transmission bars have the same density ρ and have the same cross-sectional area A. The striker bar in this figure has a different density ρ_{st} than the incident and transmission bars but it has the same cross-sectional area.

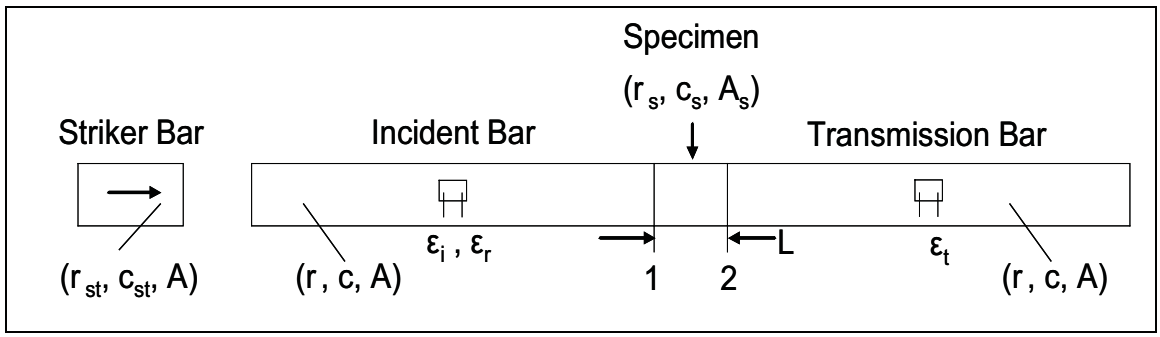

Figure 1

Illustration of SHPB Test Setup

In the figure above L is the specimen length, ε is the extensional strain in the bars, and the subscripts i, r, and t is for the incident, reflected, and transmitted pulse, and st stands for striker bar while s stands for specimen.

Objective

The objective of this investigation is to provide quality dynamic (high strain-rate) mechanical properties for a solid grade severe-weather (SW) brick and to illustrate the need for careful evaluation of the strain-rate effects on geomaterials.

Topics Covered in Thesis

The purpose of this thesis is to provide dynamic material property data for a solid grade SW brick using a modified SHPB technique. Chapter Two contains a literature review of previous work using the SHPB and discusses test procedure modifications for testing brittle materials. Chapter Three explains the SHPB theory and the equipment used for this thesis. Chapter Four discusses the mechanical properties using results of quasi-static tests from a servo-controlled test device and dynamic tests using the SHPB. Finally, Chapter Five presents conclusions and recommendations for future work.

CHAPTER II

LITERATURE REVIEW

Introduction

Bertram Hopkinson (1914) designed the first Hopkinson bar in 1914. This test device consisted of a long steel rod (B) with a steel billet (C) attached to the end with grease and a ballistic pendulum (D) as shown in Figure 2. When the steel rod was impacted by an explosive event (see detonation cord, A), the steel billet was then sent airborne into the ballistic pendulum, which measured the maximum pressure and the duration of the event. Later, R. M. Davies (1948) added parallel-plate condensers to the steel rod to measure the strains in the steel bar (Figure 3). From the condenser data, the pressure time-histories were plotted based on Davies' assumptions that the displacement in the bar was proportional to the pressure in the bar and that the elastic limit of the bar material was not exceeded during the test.

Herbert Kolsky (1949, 1963) further improved the Hopkinson bar test by sandwiching the test specimen between two steel bars and measuring the strains in both bars. This device, shown in Figure 4, contains three bars (striker bar, incident bar, and transmission bar) and a test specimen, and is commonly called the split Hopkinson pressure bar (SHPB) or the Kolsky bar. When the striker bar impacts the incident bar a compressive stress pulse develops and is measured using a strain gage attached at the center of the incident bar. At the specimen interface, part of the stress pulse is reflected

back into the incident bar while the rest of the pulse travels through the specimen into the transmission bar. Another strain gage is attached at the center of the transmission bar to record the transmitted stress pulse. The voltage-time data retrieved from the strain gages, such as the data displayed in Figure 5, is then used to determine the stress-strain response of the test specimen by assuming one-dimensional wave propagation theory. Gray (2000), Lindholm (1964), and Nicholas (1982) provide detailed information about the SHPB and how to determine the stress-strain response of the specimen.

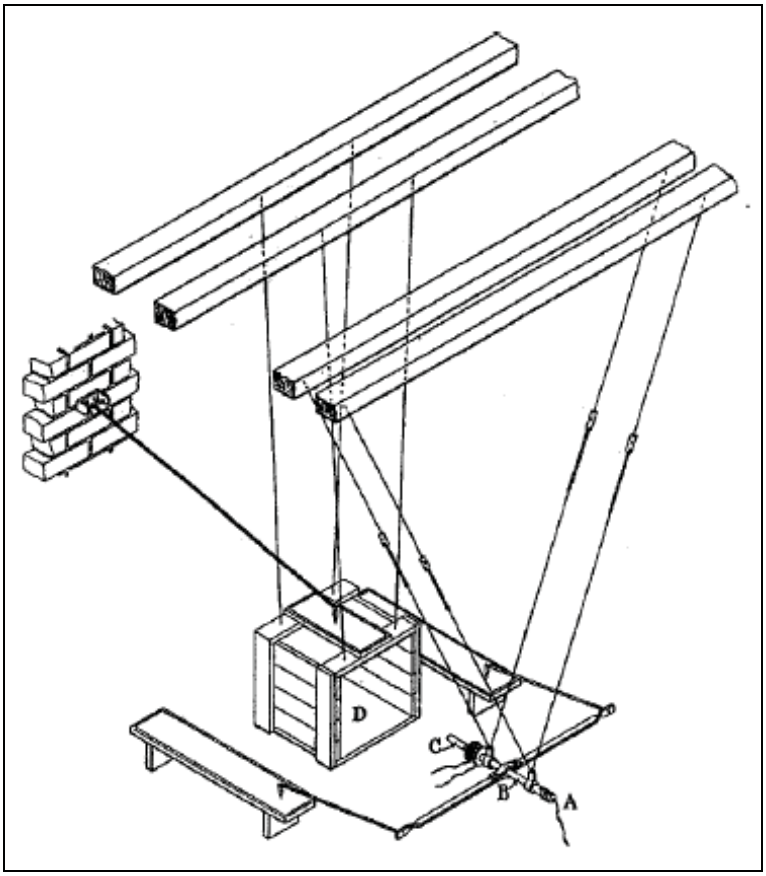

Figure 2

Original Hopkinson Bar by Bertram Hopkinson (Hopkinson, 1914)

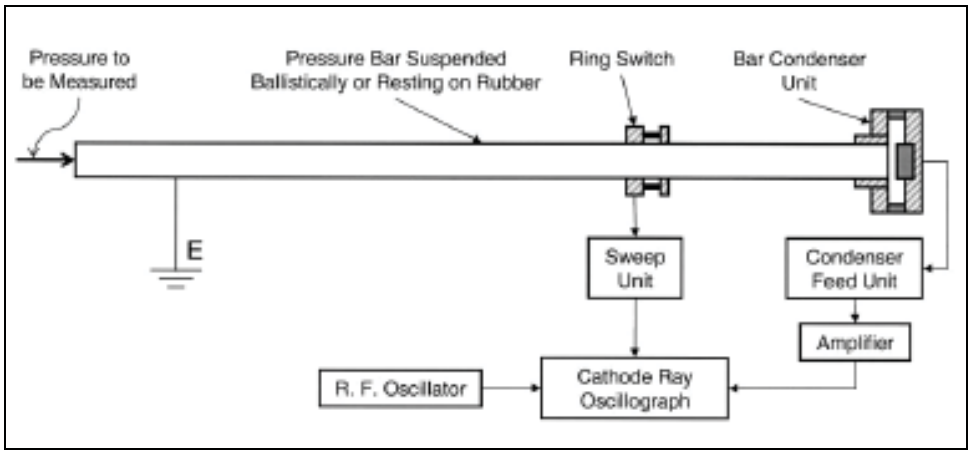

Figure 3

Hopkinson Bar with Davies Modifications (Davies, 1948)

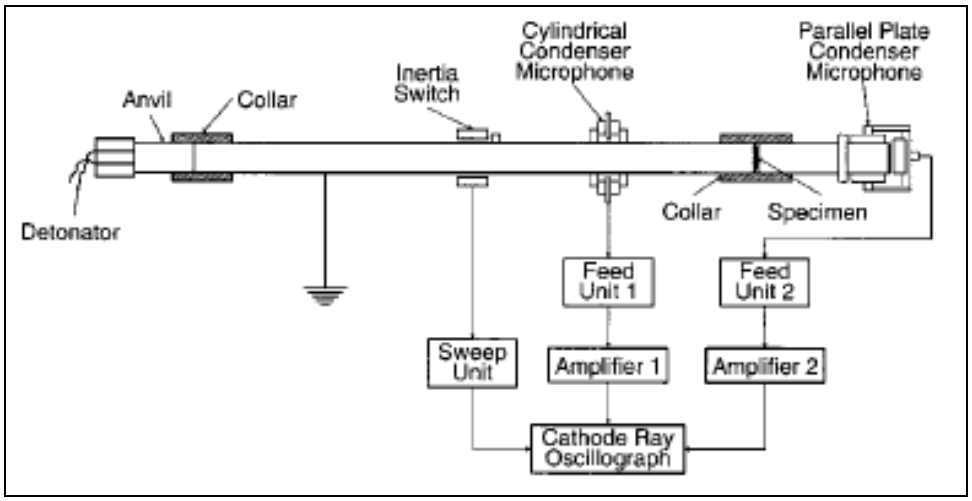

Figure 4

Kolsky's Hopkinson Bar (Kolsky, 1949)

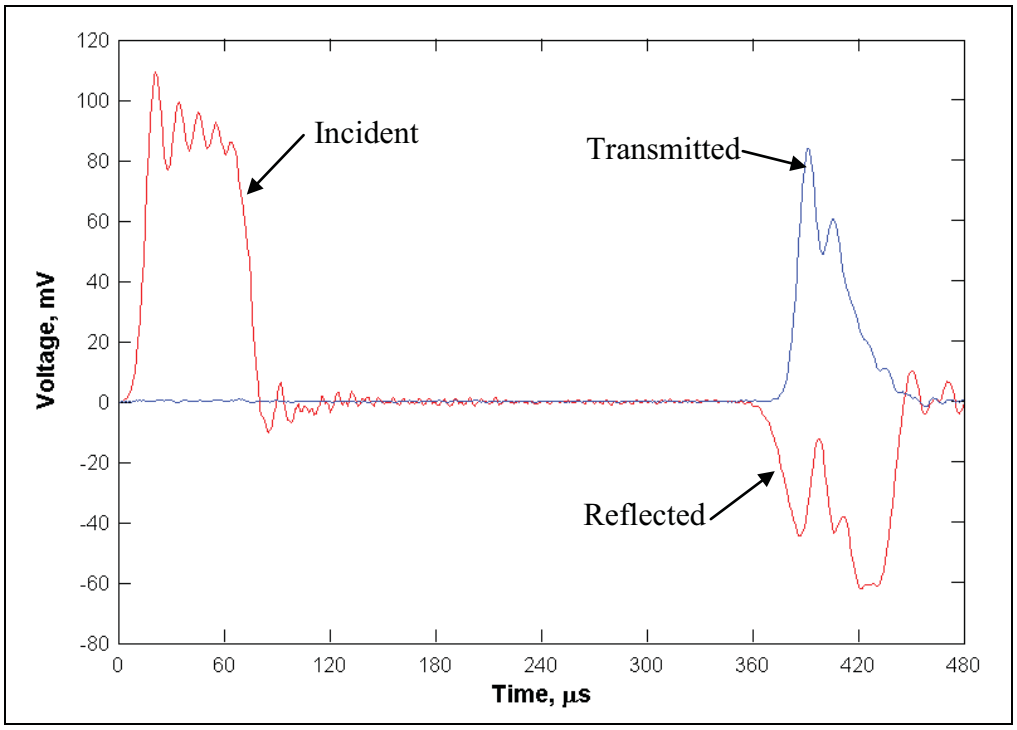

Figure 5

Voltage-Time Response from a Classical SHPB Test with a Brick Specimen

The SHPB was originally developed and has been used extensively to test the dynamic response of elastic-plastic metals, which experience significant plastic flow and large strains at strain-rates between 10^2-10^4 s^{-1} (Meyers, 1994). In the last few decades, researchers have used the SHPB to dynamically test an assortment of materials such as geomaterials and ceramics under various stress and strain conditions. Researchers have modified the SHPB to perform tensile (Ross et al., 1989), torsion (Lewis and Campbell, 1972), confined compression (Christensen et al., 1972), and elevated temperature (Gray et al., 1998) tests. These modifications involve some structural changes to the basic

SHPB. Since this thesis focus is on the dynamic compressive material property of a brick and it strain-rate effects these modifications will not be further discussed in this literature review.

Since the SHPB was originally designed to test elastic-plastic metals modifications are necessary to test brittle materials such as mortar (Schmidt and Cazacu, 2006), rock (Frew et al., 2001), concrete (Ross et al., 1989), and ceramics (Chen and Ravichandran, 1997). Modifications are necessary because brittle materials generally experience minimal amounts plastic flow prior to failure, i.e., failure often occurs at strains below one percent. This means that most brittle materials will fail before the ramp pulse in the incident bar reaches its peak amplitude. To measure the elastic and early-yield behavior for brittle materials the classical SHPB must be modified.

Modifications for Testing Brittle Materials

Many researchers have found that reducing the rise time of the initial stress (ramp) pulse will improve the quality of the mechanical response data for testing of brittle materials. To test a steel-fiber-reinforced concrete, Lok and Zhao (2004) and Lok et al. (2003) used a tapered striker bar to reduce the ramp pulse while Jicheng and Xibing (1998) used striker bars with different hemispherical ends to vary the stress pulses in the incident bar for testing rock. Another method for reducing the rise time of the stress pulse, and likely the most common method, is to add a tip material or pulse shaper to the initial impact end of the incident bar as shown in Figure 6. The pulse shaper in this figure has a cross-sectional area a_0 and a thickness of h_0.

Pulse Shapers

The history for using pulse shapers is thought to have started with Duffy et al. (1971). Duffy et al. (1971) used concentric tubes to smooth the pulses for testing 1100-0 aluminum with an explosive loading torsional split Hopkinson bar. In the last two decades, pulse shaping techniques have greatly advanced in part to the research performed by Nemat-Nasser, Isaacs, and Starrett, (1991). Nemat-Nasser et al. (1991) developed a pulse shaping model for predicting the incident bar stress with an oxygen free high purity copper pulse shaper. The pulse shaper model was produced in part with their research for testing brittle ceramic materials with the SHPB. When pulse shaping techniques such as Nemat-Nasser's et al. (1991) are used correctly, the dispersion of the ramp pulse (Wu and Gorham, 1997) is tamped, i.e., high frequency oscillations of the stress pulses do not occur, as shown in Figure 7, and dispersion correction formulas, such as the one used by Tang et al. (1992), based on the Fourier transform used by Follansbee and Frantz (1983) for dispersion correction, are not necessary.

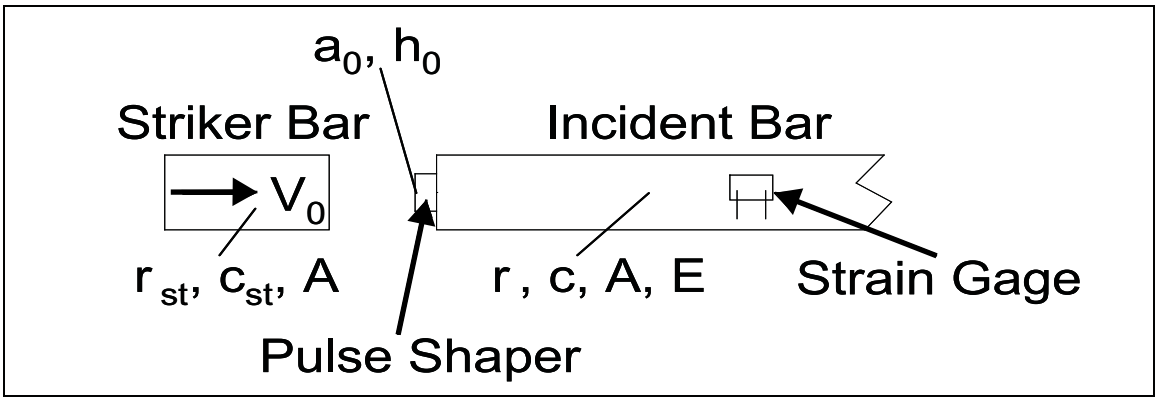

Figure 6

Initial Impact Region of a SHPB with a Pulse Shaper

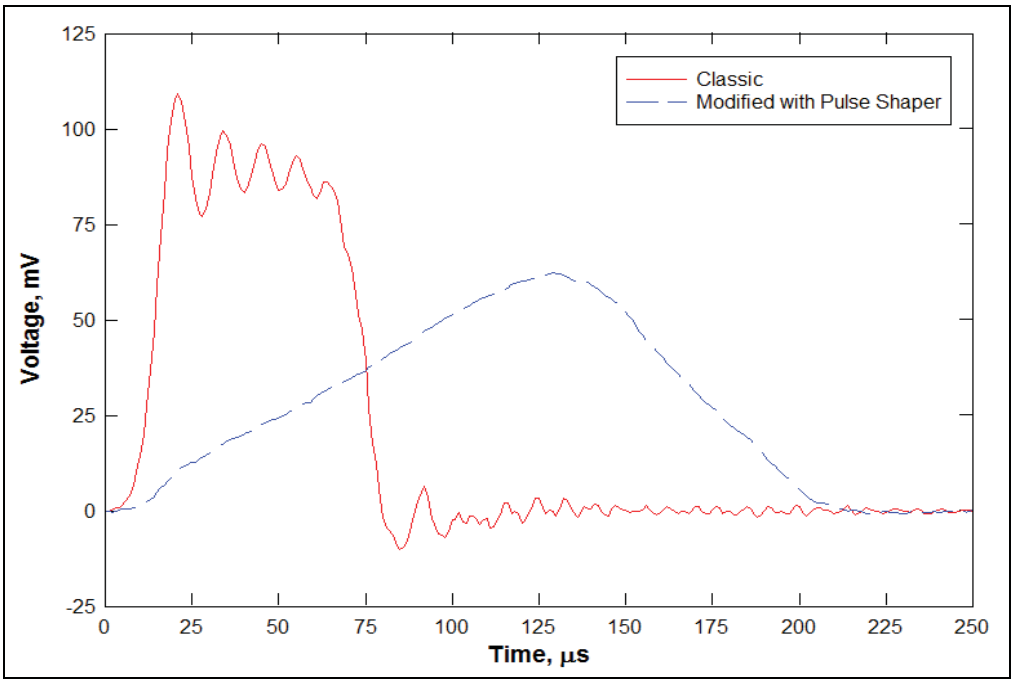

Figure 7

Initial Stress Pulse Response from a Classical and Modified SHPB Test

Many materials can be used as a pulse shaper when testing with the SHPB. Commonly, when testing metals, the pulse shaper will be the same metal material as the tested material. This is likely because the researcher already has the material to make the pulse shaper and because most of the metals tested with the SHPB exhibit elastic-plastic behavior which means the material will deform elastically upon impact. Researchers such as Nemat-Nasser et al. (1991), Chen et al. (2002), Frew et al. (2002), and Song et al. (2007) have effectively used copper pulse shapers for testing brittle materials. Copper is frequently used for pulse shapers because of ductile behavior upon impact. The annealed C11000 copper pulse shapers used in this thesis were chosen based on data from Danny Frew's (2001) dissertation, in which Frew developed and tested a pulse shaping model program using this material.

Bar Material

Another modification of the conventional SHPB in this thesis was to use a high-strength aluminum alloy instead of the more conventional maraging steel for the incident, transmission, and striker bars. The high-strength aluminum alloy has an impedance that is lower than that of maraging steel. Chen et al. (1999) and Gray and Blumenthal (2000) found that the lower impedance of the aluminum bars increases the amplitude of the signal transmission of the stress pulse within transmission bars. In general, when there is a large mismatch between the impedance of the incident bar material and that of the test specimen as there is with brick, most of the stress pulse is reflected back into the incident bar. This causes the amplitude of the stress pulse transmitted through the specimen into the transmission bar to be minimal and in some cases the amplitude of the recovered signal can be less than the noise produced by the strain gage reporting the signal. Therefore using aluminum bars when testing low impedance materials is advantageous for analyzing data from low-strength, low-impedance materials such as brick.

Specimen Shape and Size

SHPB specimens are generally right-circular cylinders with flat and parallel loading faces. On occasion, depending on the material being tested and the type of SHPB test, researchers have used cubic and dog-bone shaped specimens. Since brick is easy to dynamically fail under compression, right-circular, cylindrical specimens with a length-to-diameter (L/D) ratio of 1 were used in this thesis. Frantz et al. (1984) and Gray (2000) discussed previous research in which it was determined that the radial and longitudinal inertia is minimized and the end friction effects are reduced with an L/D ratio ranging from 0.5 to 1. Based on the frictional effects between the bars and the specimen when

using a short specimen and that the magnitude of the transmitted strain pulse is maximized when the specimen and bar diameters are equal as discussed by Frew et al. (2001), a L/D ratio of 1 was selected for testing the brick.

CHAPTER III

SPLIT HOPKINSON PRESSURE BAR TESTING TECHNIQUE

Introduction

Kolsky (1949, 1963) not only developed the device that is considered the classical SHPB, he also was the first to present the equations for calculating specimen properties from the strain histories in the incident and transmission bars. These equations were derived from the classical equation for one-dimensional wave propagation in elastic bars and assumed that the specimen is in dynamic stress equilibrium during the test and is loaded at a constant strain-rate for the duration of the test. In this chapter, the SHPB theory is explained, and the equipment described.

Basic Theory

The equations for determining strain, stress, and strain-rate for the SHPB have been documented by many researchers, but this thesis uses the equations documented by Nicholas (1982). All of the equations are based on the assumption that the incident and transmission bars have the same constant cross-sectional area A, Young's modulus E, and density ρ. In addition, stress is defined as positive in compression while strain is positive in tension, velocities are positive in the positive x-direction, and the specimen is in a uniaxial stress state.

In general the, displacement of the bar is defined as

$$u = c\int_0^t \varepsilon\, dt \tag{3}$$

were u is the displacement at time t, c (equation 2) is the elastic wave velocity in the bar, and ε is extensional strain.

Equation 3 can be used to determine the displacements on both ends of the specimen referred to as u_1 and u_2 (Figure 8). The displacement of the specimen at 1 is due to the incident and reflected pulses, ε_i and ε_r, and is calculated as

$$u_1 = c\int_0^t (\varepsilon_i - \varepsilon_r)\, dt \tag{4}$$

while the displacement of the specimen at 2 is due to the transmitted pulse, ε_t, is

$$u_2 = c\int_0^t \varepsilon_t\, dt \ . \tag{5}$$

The average strain in the specimen can be written in terms of the displacements as:

$$\varepsilon_s = \frac{u_1 - u_2}{L} \tag{6}$$

or in terms of the strain pulses as

$$\varepsilon_s = \frac{c}{L}\int_0^t (\varepsilon_i - \varepsilon_r - \varepsilon_t)\, dt \tag{7}$$

where L is the specimen's length.

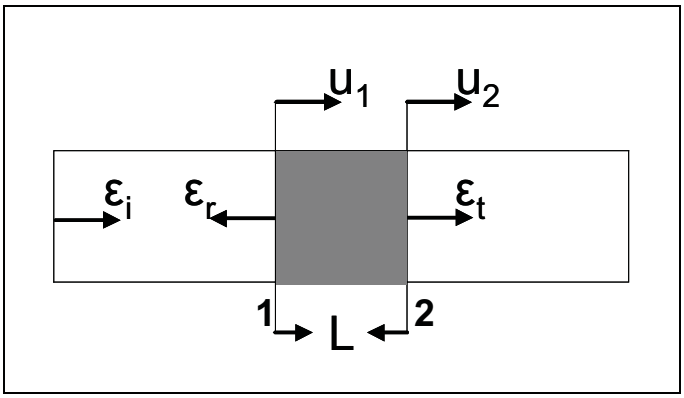

Figure 8

Incident Bar, Specimen, and Transmission Bar

The forces applied to the ends of the specimen are determined from the elastic response of the incident and transmission bars.

$$P_1 = EA(\varepsilon_i + \varepsilon_r) \tag{8}$$

$$P_2 = EA\varepsilon_t \tag{9}$$

where E is the Young's modulus, A is the cross-sectional area of the bars. The average force is

$$P_{avg} = \frac{EA}{2}(\varepsilon_i + \varepsilon_r + \varepsilon_t) \tag{10}$$

Since Kolsky's SHPB method (Kolsky, 1949, 1963) assumes that the specimen is under dynamic stress equilibrium, the forces applied to the ends of the specimen are equal, i.e., $P_1=P_2$. Equations 8 and 9 can be simplified into

$$\varepsilon_i + \varepsilon_r = \varepsilon_t \tag{11}$$

and substituting for ε_i in equation 7 gives,

$$\varepsilon_s = \frac{c}{L}\int_0^t (\varepsilon_t - \varepsilon_r - \varepsilon_r - \varepsilon_t)\,dt\,. \tag{12}$$

For a specimen in dynamic stress equilibrium with the cross-sectional area of A_s, the stress, strain, and strain-rate for the specimen are

$$\sigma_s = E\frac{A}{A_s}\varepsilon_t \tag{13}$$

$$\varepsilon_s = \frac{-2c}{L}\int_0^t \varepsilon_r \, dt \tag{14}$$

$$\dot{\varepsilon}_s = \frac{-2c}{L}\varepsilon_r \, . \tag{15}$$

Equipment

The SHPB at the U.S. Army Engineer Research and Development Center (ERDC) that was used for this thesis work is shown in Figure 9. This SHPB uses a gas gun to propel the striker bar into the incident bar. The striker, incident, and transmission bars were all machined from 7075-T6 aluminum (see Table 1 for material properties). Both the incident and transmission bars had a diameter of 19 mm and were 1829 mm in length. The two striker bars (Figure 10) had diameters of 19 mm, but one was 76 mm in length while the other was 152 mm in length. To perform an ideal test with the SHPB, the incident and transmission bars should be straight, free to move axially, and aligned with each other and the center of the barrel of the gas gun. Prior to each test, the striker bar is placed into the gun barrel and then aligned inside the gun barrel with the incident bar by blue nylon sabots (Figure 10).

Table 1

Material Properties for the Striker, Incident, and Transmission Bars

Material Properties	**Values**
Young's modulus, *E*	72 GPa
Density, ρ	2810 kg/m^3
Elastic wave velocity, *c*	5062 m/s

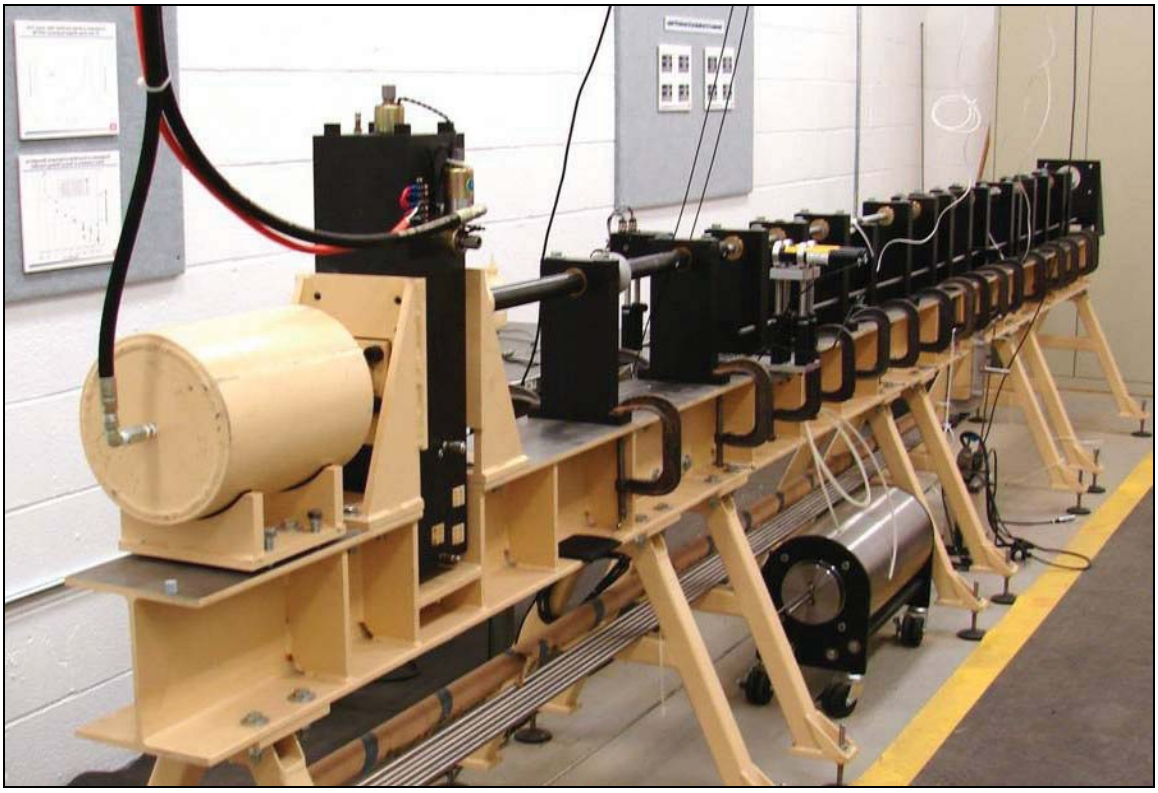

Figure 9

Photograph of the SHPB at ERDC

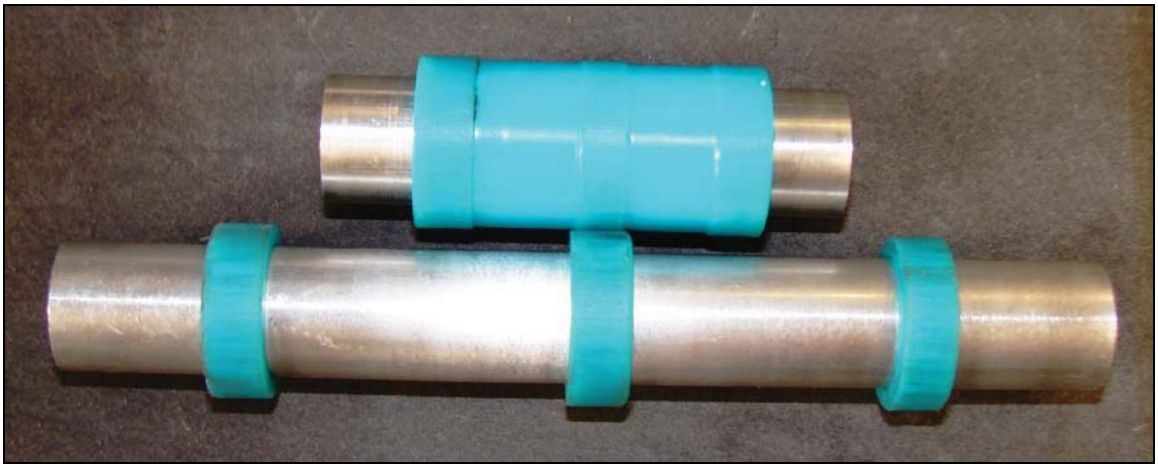

Figure 10

The Striker Bars Used During Testing

The initial impact velocity of the striker bar with the incident bar was determined by using two 0.8-mW helium-neon lasers and two photo detector units (Figure 11). To determine the velocity, the distance between the lasers were measured and then divided by the time difference in which the first laser and the second laser are disrupted by the striker bar. The time difference was recorded by a two-channel 100 MHz Tektronix TDS220 digital oscilloscope. In addition, the first laser was used to trigger the four-channel Tektronix 420A digitizing oscilloscope to record the strains from the incident and transmission bars.

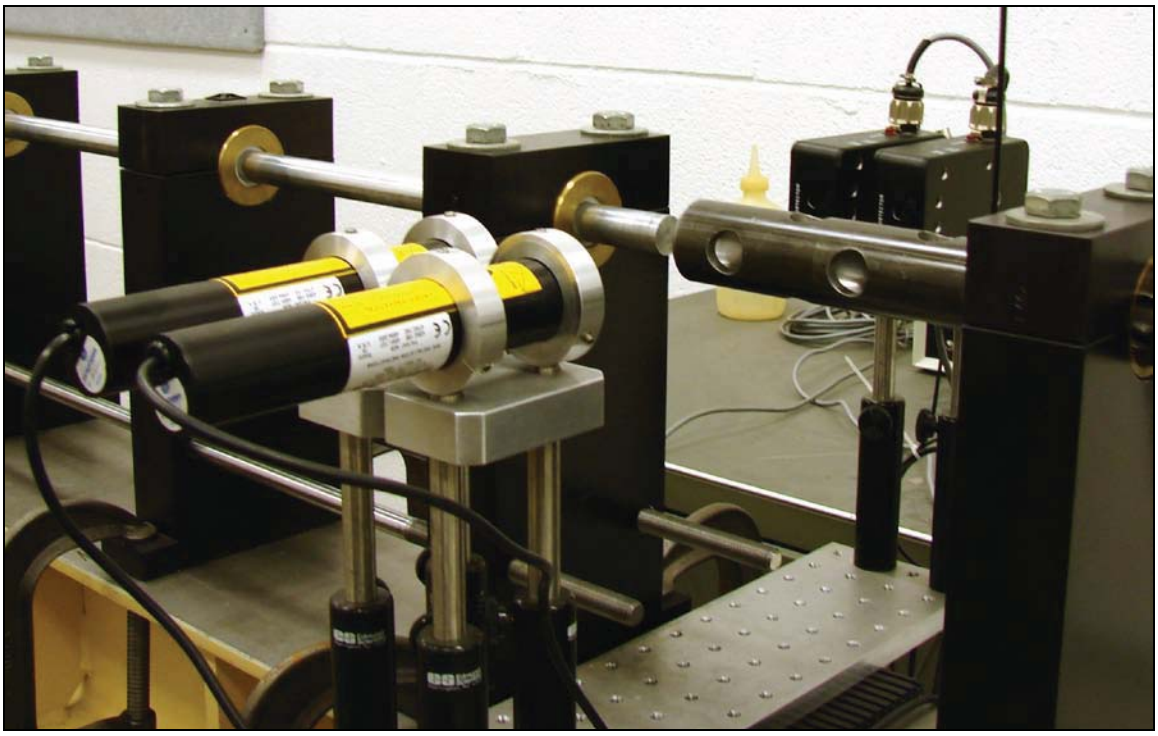

Figure 11

Photograph of the Lasers and Photo Detectors

The strains recorded by the four-channel Tektronix 420A digitizing oscilloscope are from strain gages on the incident and transmission bars that were located approximately 915 mm from the test specimen at the middle of each bar. The 1000-ohm strain gages, produced by Measurements Group, Inc., form part of two Wheatstone half-bridges on each bar and are excited by a 30-volt DC Hewlett Packard E3611A power supply. Prior to being recorded by the oscilloscope, the transmitted signal from the gages are amplified with a ADA400A differential preamplifier.

The last piece of equipment involved in this test series was the pulse shaper illustrated in Figure 6. All the pulse shapers were made from C11000 copper that was heat treated for 2 hours at 427˚C to anneal the material. The annealed C11000 copper

was used because it is very ductile and will plastically deform upon loading. The sizes of the pulse shapers ranged in diameter from 3.97 to 9.53 mm and ranged in thicknesses from 1.59 to 12.70 mm. Different diameters and thicknesses were necessary to perform experiments at various strain-rates. Frew's (2001) pulse shaper model program was used to determine the pulse shaper dimensions for the tests discussed in this thesis. Frew's (2001) pulse shaper model program uses the material properties and dimensions of the pulse shaper, striker bar, and incident bar, as well as the predicted striker bar velocity to determine the incident bar stress. Generally a good pulse shaper will produce a fairly linear initial incident stress loading as seen in Figure 12. The results of all the SHPB tests with and without pulse shapers are discussed in the next chapter.

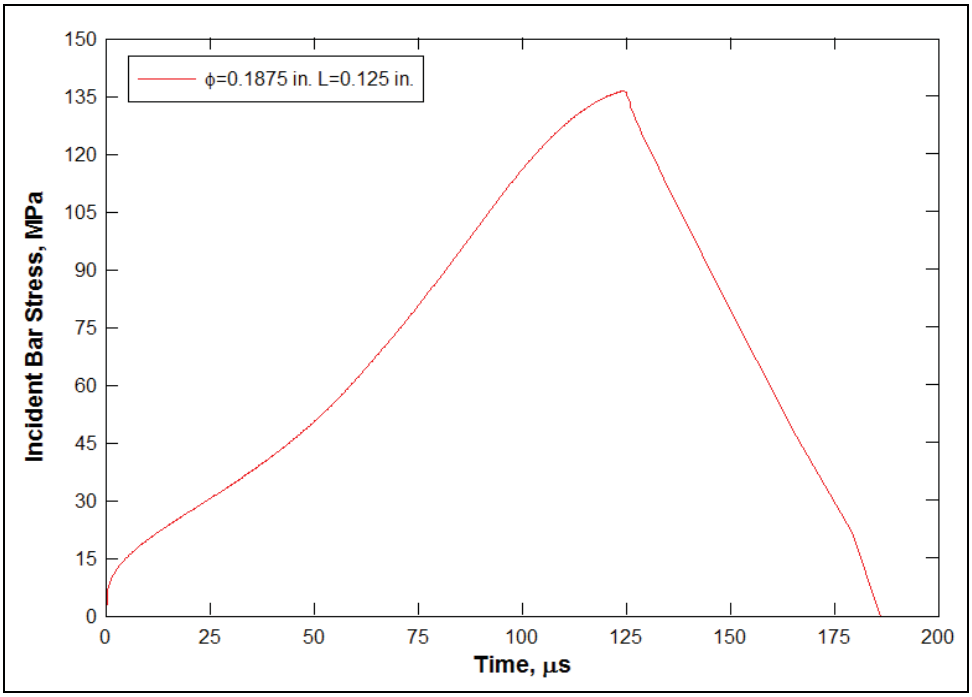

Figure 12

Aluminum Incident Bar Prediction Result for an Annealed C11000 Copper Pulse Shaper at the Striking Velocity of 30 m/s

CHAPTER IV

ANALYSIS OF EXPERIMENTAL DATA

Introduction

This thesis uses the same solid grade SW brick that was documented by Williams et al. (2005). In this chapter, results from the quasi-static tests reported by Williams et al. (2005) and the dynamic tests from the SHPB for the brick are discussed.

Quasi-Static Stress-Strain Data

Williams et al. (2005) performed a series of quasi-static compression tests on cylindrical specimens cored vertically from the center of 10.16 cm by 6.35 cm by 20.32 cm extruded solid grade SW bricks (Figure 13). These bricks meet or exceed the requirements under American Society for Testing and Materials (ASTM) standard C 902-09 (ASTM, 2009a) and are considered to be pedestrian and light traffic paving brick. Since SHPB tests are dynamic unconfined compression tests, only the quasi-static unconfined compression tests performed by Williams et al. (2005) will be discussed in this thesis. The unconfined compression tests were performed at a nominal strain-rate of 10^{-5} s^{-1} following the ASTM standard C 39-05 (ASTM, 2009b). The physical properties of these test specimens are in Table 2, and the quasi-static test results are in Figure 14. The principal stress difference, q, shown in Figure 14 in equation form is,

$$q = \frac{\text{Axial Load}}{A_o(1-\varepsilon_r)^2} \tag{16}$$

where A_o is the original cross-sectional area and ε_r is the radial strain. The radial strain, ε_r, was computed by dividing the measured radial deformation, Δd (change in diameter), by the original diameter, d_o, i.e., $\varepsilon_r = \Delta d/d_o$. The axial strain, ε_a, was computed by dividing the measured axial deformation, Δh (change in height), by the original height, h_o, i.e., $\varepsilon_a = \Delta h/h_o$ (Williams et al., 2005). Williams et al. (2005) reported that no attempt was made to capture the post-peak stress-strain behavior after failure for the unconfined compression tests. A compressive strength of 73 MPa was calculated by averaging the peak principle stress differences of the four quasi-static tests. The compressive strength resulting from these tests provide a baseline to which the dynamic SHPB test data can be compared. Note, the equations discussed in this section are valid for the quasi-static tests and do not apply for the SHPB tests.

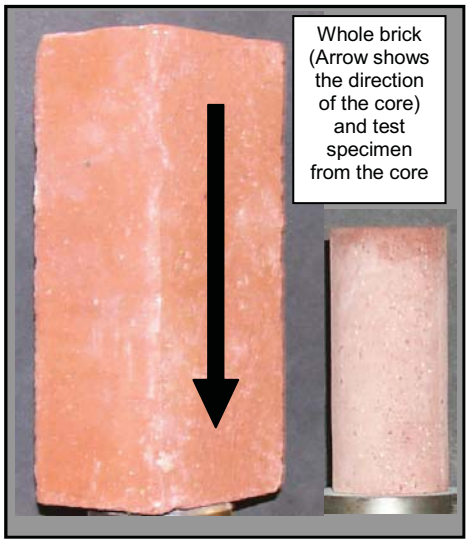

Figure 13

Solid Grade SW Brick

Table 2

Quasi-Static Unconfined Compression Test Specimen's Physical Properties and Compressive Strength

Test ID	Compressive Strength, MPa	Specimen Diameter, mm	Specimen Length, mm	L/D	Weight, g	Wet Density, kg/m^3
01	67	49.35	112.42	2.28	423.02	1967.04
02	81	49.61	110.47	2.23	429	2009.43
03	76	49.43	108.76	2.2	415.45	1990.65
04	69	49.43	112.34	2.27	425.51	1973.86
Average	73	49.46	111	2.24	423.25	1985.25

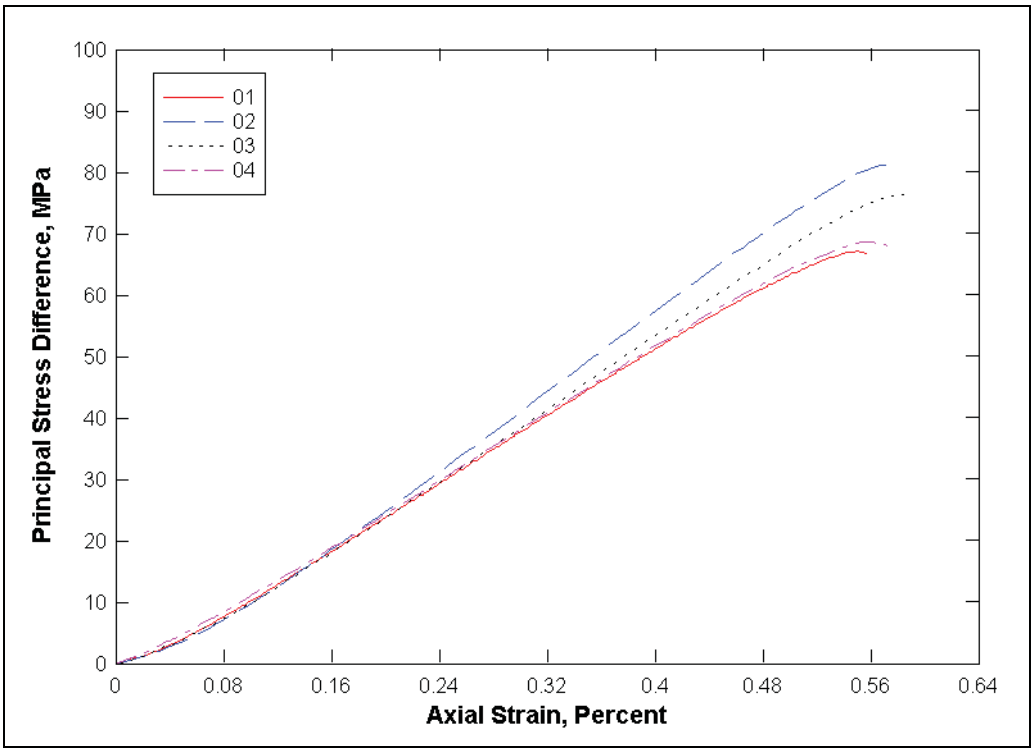

Figure 14

Quasi-Static Unconfined Compression Stress-Strain Data (Williams et al., 2005)

Dynamic Stress-Strain Data

Classical Dynamic Data

The dynamic unconfined stress-strain behavior of the brick at intermediate strain-rates (10^0-10^3 s^{-1}) were determined by performing four SHPB experiments. All of the SHPB specimens were circular cylinders with a nominal diameter and length of 19 mm for a L/D of 1. Specimens with a L/D of 1 were used because the test specimens must be short enough so that a uniform state of stress can be achieved during loading along the specimen length but long enough so that friction between the surfaces of the specimen ends and the bars does not significantly affect the specimen's strength. Table 3 lists each of the classical SHPB test specimen's physical properties, L/D ratio, and the velocity of the striker bar. The velocity of the striker bar is included in Table 3 because it is generally assumed that as the impact velocity between the striker and incident bars increase so will the strain-rate. Changes in the striker bar length and material as well as the use of a pulse shaper can affect the velocity/strain-rate assumption.

The voltage-time response of a classical SHPB test with a brick specimen is shown in Figure 15. This figure shows the incident, reflected, and transmitted responses from test specimen 4A (see Table 3 for specimen properties). The ramp pulse in the incident bar displays a fast rise time of about 18 μs. The stresses, determined by the forces calculated using equations 8 and 9, and average strain-rate, derived from equation 7, are plotted versus time for test 4A in Figure 16. The Kolsky SHPB method (Kolsky, 1949 & 1963) assumes that the SHPB specimen is in dynamic equilibrium during the experiment and deforms at a constant strain-rate during most of the test. For

test 4A, the stresses (σ_1 and σ_2, see Figure 1 for location of 1 and 2 notation) that are determined at each end of the test specimen shown in Figure 16 do not agree and display high-frequency oscillations cause by dispersion in the incident and transmission bars. Since the stresses do not agree the test specimen lacks dynamic stress equilibrium during the test. Additionally, the strain-rate data shown in Figure 16 also displays high-frequency oscillations that results in data from which a constant strain-rate cannot be determined. Since both of the assumptions Kolsky based his SHPB method on are violated, no quality material properties can be determined from this test. The results of the three other classical tests (1A, 2A, and 3A) displayed similar trends as that shown in Figures 15 and 16. See Appendix A for the voltage-time response for tests 1A, 2A, and 3A.

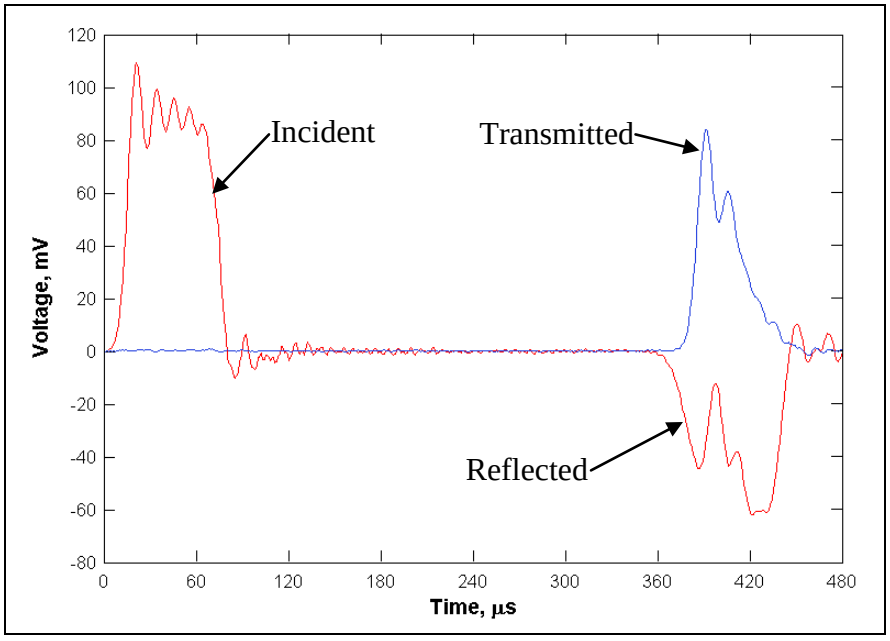

Figure 15

Voltage-Time Response from Classical SHPB Test 4A for a Brick Specimen

Table 3

Classical SHPB Test Specimen's Physical Properties and Impact Velocity of the Striker Bar

Test ID	Specimen Diameter, mm	Specimen Length, mm	L/D	Weight, g	Wet Density, kg/m^3	Striker Velocity, m/s
1A	18.77	19.26	1.03	10.40	1951.25	12.83
2A	18.83	19.13	1.02	10.22	1918.75	19.70
3A	18.74	19.29	1.03	10.39	1952.88	24.67
4A	18.67	19.23	1.03	10.40	1975.67	28.87

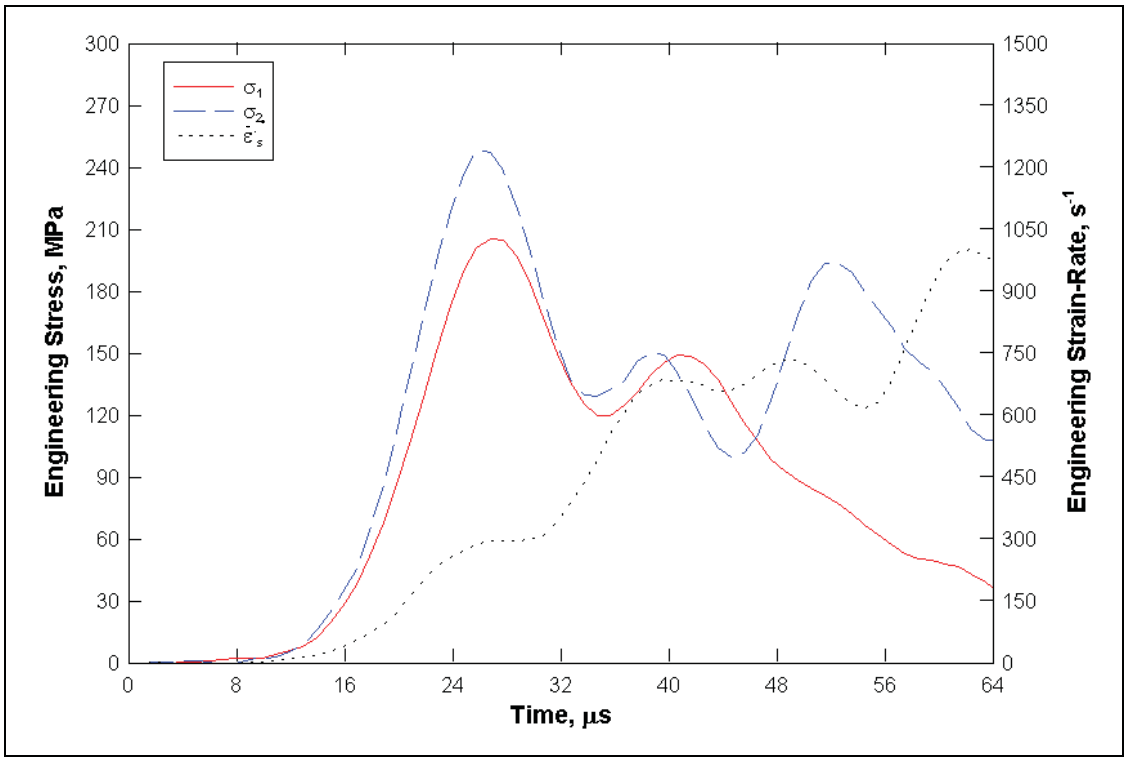

Figure 16

Interface Stresses and Strain-Rate from Classical SHPB Test 4A for a Brick Specimen

Figure 17 displays the four classical SHPB tests stress-strain responses calculated from equations 13 and 14. These tests exhibit typical behavior of SHPB tests lacking

dynamic stress equilibrium and constant strain-rate, i.e., fast rise times and high-frequency oscillations caused by dispersion. Since these tests all violate Kolsky's basic assumptions for the SHPB method, the peak stress responses shown in Figure 17 cannot be related to dynamic peak compressive strength response to brick. Modifications to the SHPB are necessary for determining dynamic material properties and the strain-rate effects for this brick. In this thesis the SHPB tests will be modified through the use of a pulse shaper.

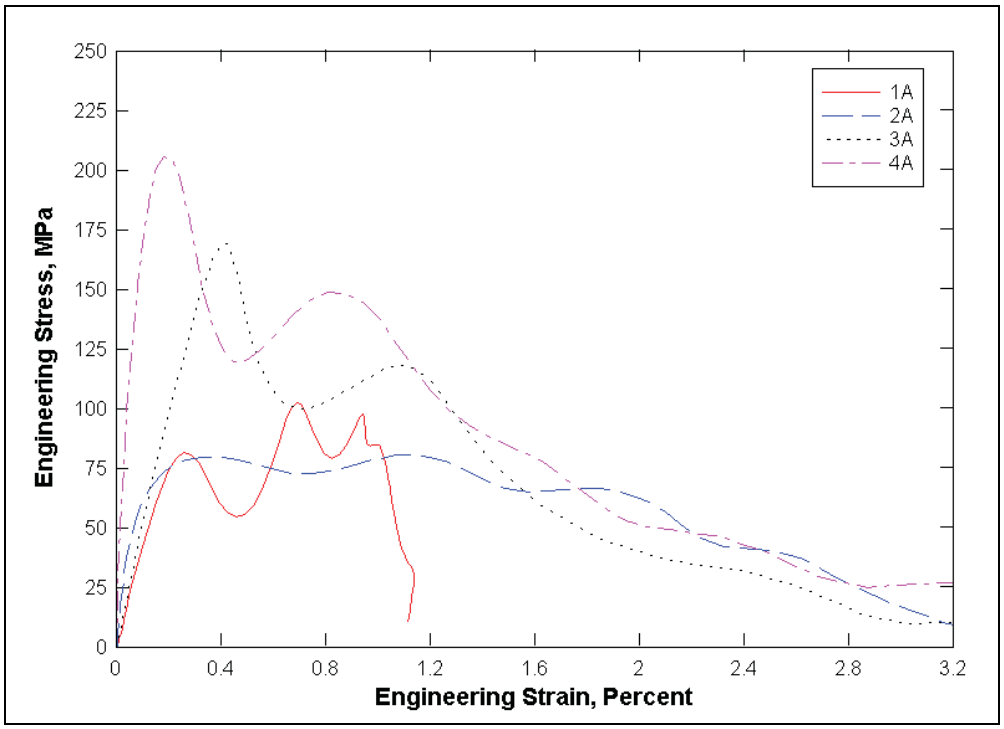

Figure 17

Stress-Strain Responses from Classical SHPB Tests with Brick Specimens

Pulse-Shaped Dynamic Data

To achieve dynamic stress equilibrium and an almost constant strain-rate during most of the specimen loading, a cylindrical annealed C11000 copper pulse shaper was

placed on the initial impact end of incident bar. When the striker bar impacts the pulse shaper the pulse shaper plastically deforms and produces a stress pulse that lengthens and removes most high-frequency oscillations from the ramp pulse in the incident bar. After the initial impact, the pulse shaper is either destroyed or losses contact with the incident bar. Therefore, the only affect the pulse shaper has is to the ramp pulse in the incident bar. In this thesis, the pulse shaper's dimensions were adjusted for each experiment according to the size and the predicted impact velocity of the striker bar using Frew's (2001) pulse shaping model program. Table 4 lists the dimensions of the pulse shapers along with the striker bar length and impact velocity for the modified SHPB tests.

Table 4

Impact Data and Pulse Shaper Dimensions

Test ID	Striker Length, mm	Striker Velocity, m/s	Pulse Shaper Diameter, mm	Pulse Shaper Length, mm
1B	152.40	28.29	4.77	3.17
2B	152.40	24.44	4.78	3.15
3B	152.40	25.77	5.72	3.80
4B	152.40	47.04	9.53	6.32
5B	152.40	42.33	9.53	3.15
6B	152.40	50.30	9.53	4.75
7B	76.20	38.78	7.16	1.59

The effect of using pulse shapers is shown using the voltage-time response data from test 3B in Figure 18. This figure displays a trapezoidal response that is common for SHPB tests that have been properly modified by a pulse shaper. The initial rise time of the ramp pulse is 125 μs, which is almost seven times greater than the ramp pulse shown in Figure 15. In addition to reducing the magnitude of the ramp pulse, the pulse shaper

eliminated the high-frequency oscillations in the ramp pulse and therefore made dispersion correction of the data unnecessary.

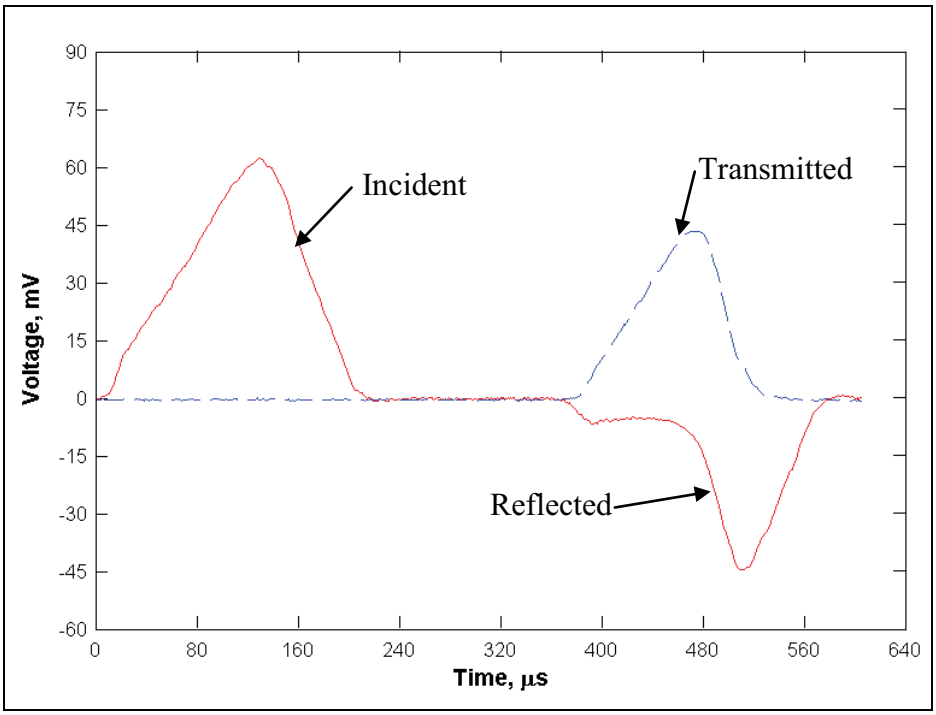

Figure 18

Voltage-Time Responses for a Modified SHPB Test with a Brick Specimen

Figure 19 displays the stress waves (σ_1 and σ_2) from each end of the test specimen for the modified SHPB tests 1B, 2B, and 3B. The stress waves from each end of test specimens 1B and 2B are almost perfectly overlapping, while the initial stress waves from each end of test specimen 3B overlap. This overlap of the stress waves illustrates that the specimens are in dynamic stress equilibrium. In this figure these tests represent the modified SHPB tests with the lowest strain-rates, which were 50, 61, and 61 s^{-1} for 1B, 2B, and 3B, respectively. To better compare the modified SHPB test Table 5 lists each test and provides the strain-rate, peak compressive strength, and physical properties

of the specimens. Interestingly, 2B and 3B have the same strain-rates. From Table 4 it is known that the same striker bar and similar velocities were used for these tests but different pulse shapers were used. By comparing the data in Figure 19 for these two tests it can be seen that pulse shaper used in 2B likely produced the more consistent stress waves.

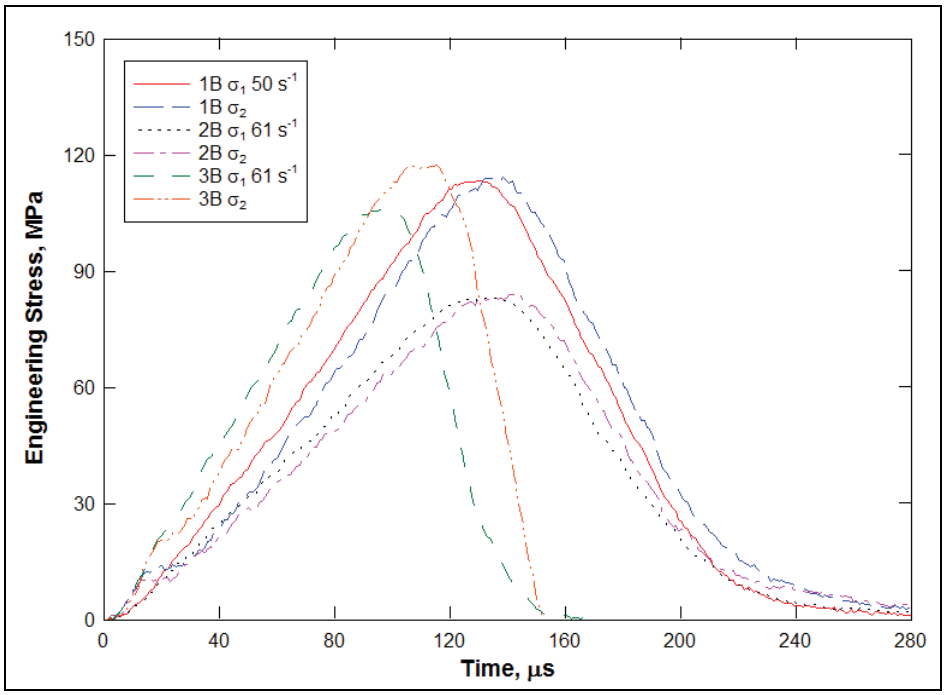

Figure 19

Stress-Time Responses of Brick for the Strain-Rates of 50 to 61 s^{-1}

Figure 20 displays the stress waves from each end of the test specimen for the modified SHPB tests 4B, 5B, 6B, and 7B. The stress waves in this figure are not as consistent for each end of the test specimen as the stress waves in Figure 19. Since the stress waves are initially similar, in this thesis these tests will be considered to be in dynamic stress equilibrium. Tests 5B and7B both display some oscillation of the stress

wave at 2. This is a result of the strain-rate of the tests, which were 206 and 101 s^{-1}, for 5B and 7B, respectively, and the pulse shapers used for these tests to ramp the initial stress pulse. The pulse shaper is assumed to be partly to blame for the oscillations since test 4B does not display oscillations but has a greater strain-rate (111 s^{-1}) than that of test 7B. For the four tests shown in Figure 20 the strain-rates ranged from 83 to 206 s^{-1} and are listed for each test in Table 5. The difference between the stress waves in Figure 20 for a given test is much greater than in Figure 19. It appears from these figures that the lower strain-rates, i.e., approximately 61 s^{-1} and below (see Figure 19), produced more consistent data in which the stress waves are more alike and there are no oscillations in the test data.

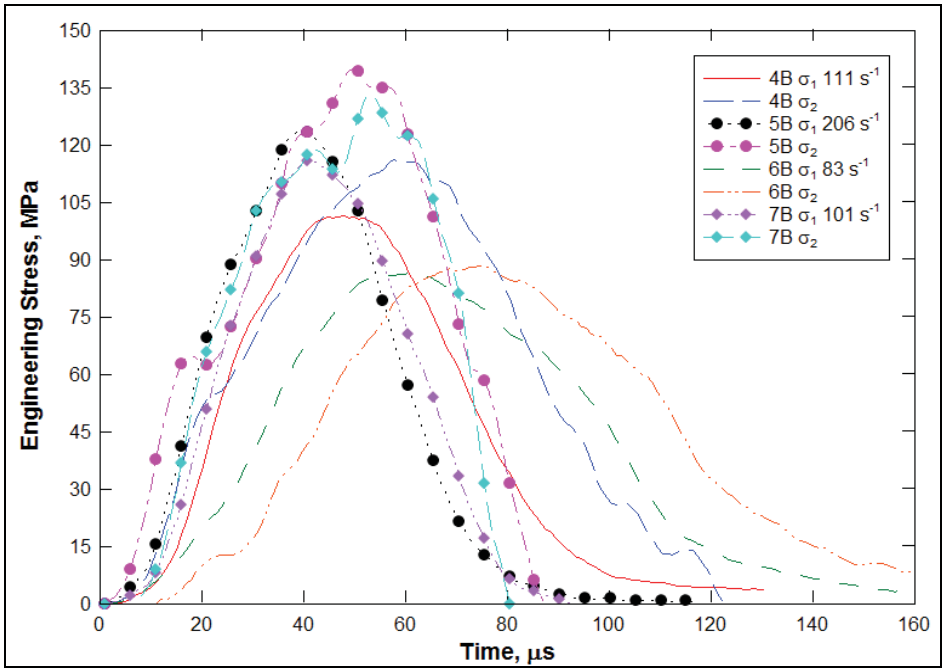

Figure 20

Stress-Time Responses of Brick for the Strain-Rates of 83 to 206 s^{-1}

Table 5

Modified SHPB Test Specimen's Physical Properties, Strain-Rates, and Compressive Strength

Test ID	Strain-rate, s^{-1}	Dynamic Compressive Strength, MPa	Specimen Diameter, mm	Specimen Length, mm	L/D	Weight, g	Wet Density, kg/m^3
1B	50	113.41	18.65	19.28	1.03	10.34	1962.83
2B	61	83.40	18.66	19.28	1.03	10.31	1955.54
3B	61	105.95	18.72	19.23	1.03	10.39	1963.33
4B	111	101.31	18.62	19.22	1.03	10.35	1978.48
5B	206	123.54	18.72	19.32	1.03	10.36	1948.65
6B	83	86.26	18.72	19.11	1.02	10.31	1959.86
7B	101	115.71	18.73	19.24	1.03	10.46	1972.58

Figure 21 is a plot of strain-rates versus time for the seven tests. The test data shows less oscillation for the lower strain-rates. The strain-rates for each test are not constant throughout the loading of the test specimen. This is a result of the dynamic nature of the experiment and because the strain-rate is calculated using an average of the incident, reflected, and transmitted pulses. Note, that the strain-rate increases exponentially after the specimen has failed. The strain-rate for each test was determined prior to failure.

As mentioned previously, the modified SHPB tests display differences in the peak stresses. To better compare the peak stress behavior of these tests, Figure 22 presents the average stress-strain responses from all of the modified SHPB tests. Test specimens 1B and 2B display a different unloading character than the other tests, which is likely a result of the failure mode of these specimens. These two test specimens split into several large pieces that were recovered after the SHPB tests were complete, while test specimens, 3B, 4B, 5B, 6B, and 7B were completely pulverized during testing. The mode of failure

appears to significantly influence the response of the material. At this time it is unknown how to cause this exact failure mode but it is likely a result of the strain-rate since this type of failure occurred during the two of the lowest strain-rates discussed in this thesis.

A dynamic increase factor (DIF) was calculated using the CEB Model Code for concrete (Comite Euro-International du Beton – Federation Internationale del la Precontrainte, 1990) that is defined as

$$DIF = \frac{f_{cd}}{f_{cs}} = \left(\frac{\dot{\varepsilon}}{\dot{\varepsilon}_s} \right)^{1.026\alpha} \quad for\ \dot{\varepsilon} \le 30 s^{-1} \tag{17}$$

$$DIF = \frac{f_{cd}}{f_{cs}} = \gamma \left(\frac{\dot{\varepsilon}}{\dot{\varepsilon}_s} \right)^{\frac{1}{3}} \quad for\ \dot{\varepsilon} \ge 30 s^{-1} \tag{18}$$

where f_{cd} is the dynamic compressive strength, f_{cs} is the static compressive strength, $\dot{\varepsilon}$ is the dynamic strain rate, $\dot{\varepsilon}_s$ is the static strain rate, and α and γ are defined constants. The stress-strain responses in Figure 22 indicate peak stresses ranging from 83.4 to 123.5 MPa. This range has a difference of almost 40 MPa. In general, most would assume that as the strain-rate increases so would the peak stress for the material. These tests do not follow that general assumption. In this test series, the test with the lowest strain-rate displays the third highest dynamic compressive strength out of all the tests. Since the peak dynamic compressive strengths do not display a clear increase with increasing strain-rate, an average peak compressive strength of all the tests was calculated (104 MPa) to compare with the quasi-static compressive strength (73 MPa). A DIF of 1.42 was calculated from the brick data using equation 18. The average peak compressive strength of the modified SHPB tests is almost 42 percent greater than the peak compressive strength from the quasi-static tests.

Another method to compare the quasi-static data and the dynamic SHPB data is to plot this data together as shown in Figures 23 and 24. Both of these figures show the peak stress-strain-rate data for brick, but in Figure 24 the strain-rate is plotted on a logarithmic to better display the differences between the quasi-static and dynamic strain-rates. It is obvious from both of these figures that this brick does experience strain-rate effects as all the dynamic SHPB tests exhibit greater peak compressive strengths than the quasi-static tests.

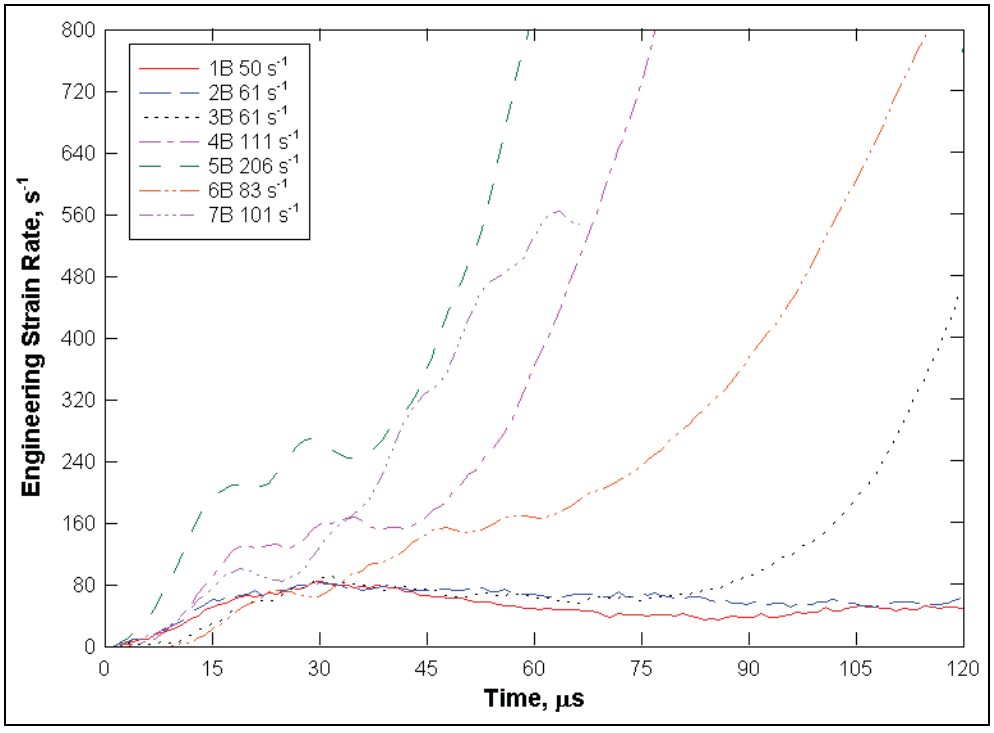

Figure 21

Strain-Rate versus Time Data from the Modified SHPB Tests on Brick

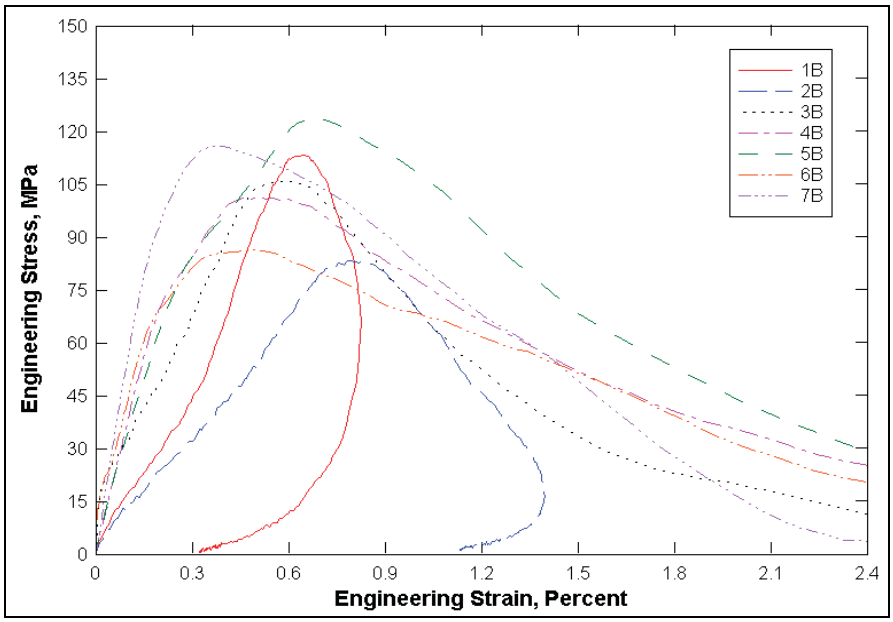

Figure 22

Stress-Strain Data from the Modified SHPB Tests on Brick

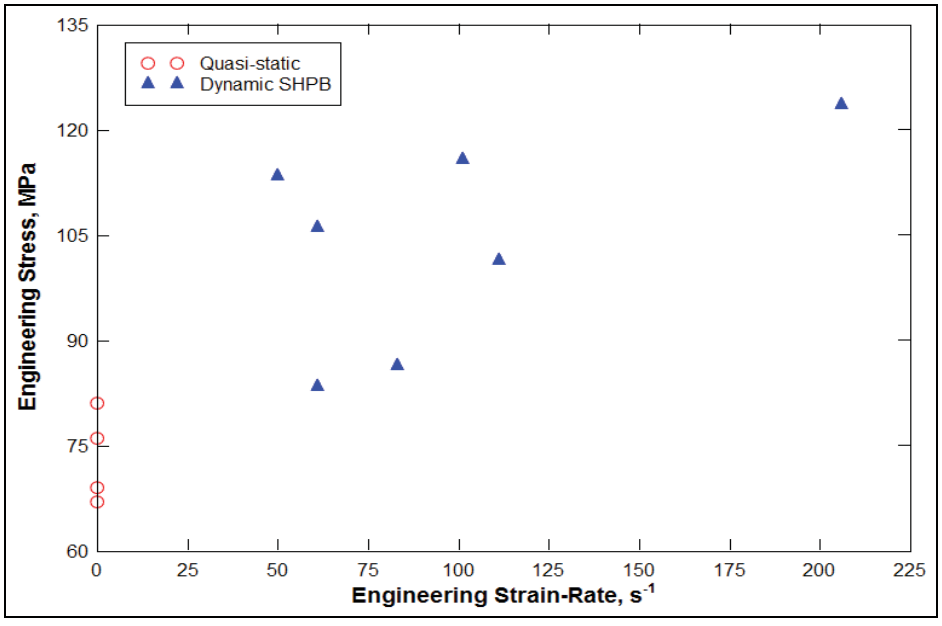

Figure 23

Peak Stress versus Strain-Rate from the Quasi-Static and Dynamic Tests on Brick

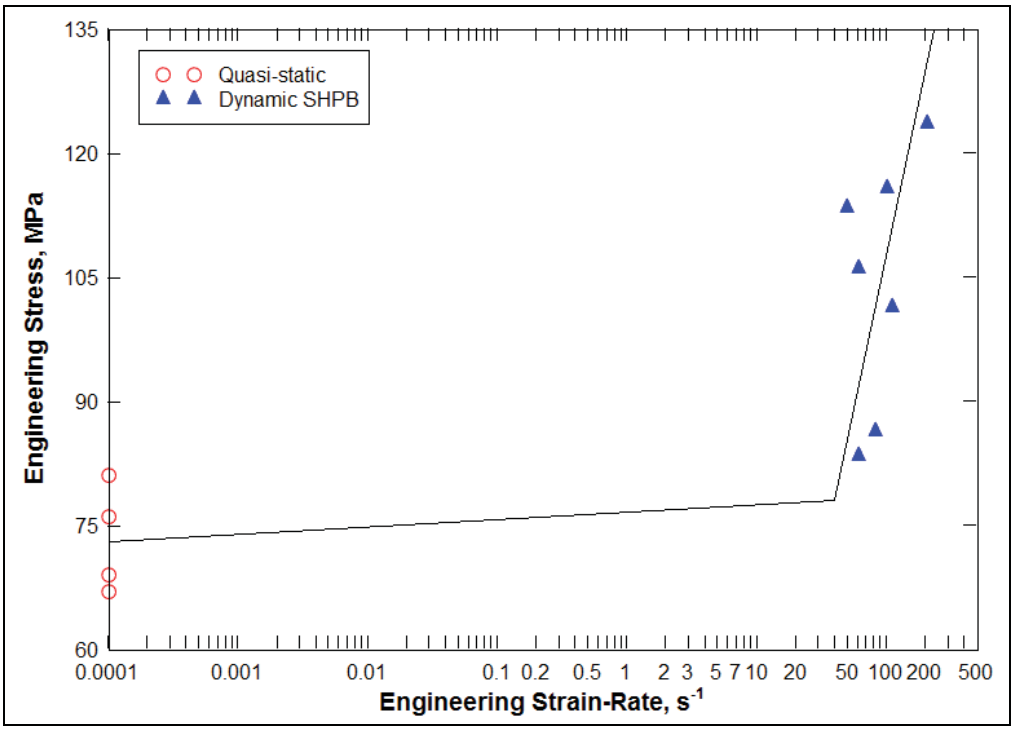

Figure 24

Peak Stress versus Log Strain-Rate from the Quasi-Static and Dynamic Tests on Brick

CHAPTER V

CONCLUSIONS AND RECOMMENDATIONS

Conclusions

This thesis used a SHPB to provide quality dynamic strength data for a solid grade SW brick for strain-rates ranging from 50 to 206 s^{-1}. Both classical and modified SHPB tests were performed. The results from the classical SHPB tests provided evidence that modifications to the SHPB are necessary when testing a brittle material such as the brick discussed in this report. These test results exhibited both a lack of dynamic stress equilibrium and constant strain-rate during the tests. With the modification of a small cylindrical copper disk at the impact end of the incident bar, the SHPB can be used to test most brittle materials. The average peak compressive strength from the seven modified SHPB tests was 104 MPa. The average compressive strength data from the SHPB tests were compared with the average quasi-static compressive strength data presented by Williams et al. (2005), and it was determined that the brick has a DIF of 1.42. This means that at high strain-rates, the compressive strength of this brick is approximately 42 percent greater than the quasi-static strength of the brick. With this information, engineers and scientists can include strain-rate effects into their constitutive models for numerical simulations of dynamic events such as high-velocity impacts and explosive detonations.

Recommendations for Future Work

The SHPB is a useful device for determining the dynamic strength properties of materials. However, the results of each test must be examined to determine if the test conforms to the assumptions that the specimen is in dynamic stress equilibrium during the test and that it is loaded at a constant strain-rate. As discussed in Chapter IV, pulse shapers were used to perform tests that comply with these assumptions. The pulse shapers were determined using Frew's (2001) pulse shaping model. Frew's pulse shaper model program is a good guideline for predicting the dimensions of the pulse shaper for a given velocity, but based on previous testing experience it does not always accurately predict the proper pulse shaper. Frew's program uses exact measurements of the pulse shaper and strike bar impact velocity for predicting the shape of the ramp pulse in the incident bar and any inconsistencies of the pulse shaper dimensions and impact velocity can affect the shape of the ramp pulse. More research into sensitivity of Frew's model for predicting the ramp pulse is recommended to improve the accuracy for selecting a pulse shaper.

Another area of interest is the effect of specimen proportions. In this thesis, it was assumed that difference in the L/D of quasi-static specimens (2.24) and the L/D of the SHPB specimens (1.03) did not affect the compressive strength of the material. Further testing of quasi-static specimens with an L/D of 1 would assist in proving or disproving the assumption. For this thesis to have completed quasi-static tests on specimens with an L/D of 1, new instrumentation for measuring the axial and radial

deformation would have been necessary. In this case, funding was not available for new instrumentation, therefore, quasi-static testing of brick specimens with a L/D of 1 was beyond the scope of this research.

Since there was not a direct correlation between the increase in compressive strength with increasing strain-rate for the range of 50 to 206 s^{-1}, more tests at the same strain-rates should be performed and if possible the future tests should include tests at greater strain-rates than achieved for this thesis. If after further tests there is still not a direct correlation between the increase in compressive strength with increasing strain-rate, specific reasons as to why this behavior occurred should be considered to better define the dynamic strength properties and the strain-rate effects for this brick. As mentioned in Chapter IV, it appears that the quality of the SHPB data is affected by the failure mode, but the peak compressive strength responses do not appear to exhibit any correlation to the failure mode. Since the failure mode of the test specimen appears not to effect the compressive strength another possibility is that there are slight differences in the composition properties of the various whole bricks used to obtain test specimens. As this was not previously a concern, two bricks were cored to produce the specimens used in this thesis, and no notation was used to distinguish the specimens. Additionally, the location from inside the brick might also be a factor in its strength. A specimen from the center of a brick might not have cured exactly the same as a specimen that is close to an edge.

For further SHPB testing, results from similar strain-rate tests for multiple bricks should be compared, and a test series should be completed comparing the test results of

specimens with similar strain-rates but from various locations inside a brick. Data from these tests will assist in determining if the brick material has a penchant for increasing compressive strength with increasing strain-rate.

REFERENCES CITED

American Society for Testing and Materials. 2009a. *Standard specification for pedestrian and light traffic paving brick.* Designation C 902-09. Philadelphia, PA: American Society for Testing and Materials.

American Society for Testing and Materials. 2009b. *Standard test method for compressive strength of concrete specimens.* Designation C 39-05. Philadelphia, PA: American Society for Testing and Materials.

Chen, W., Lu, F., Frew, D.J., and Forrestal, M.J. (2002). Dynamic compression testing of soft materials. *J. Appl. Mech.,* **69**, 214-223.

Chen, W. and Ravichandran, G. (1997). Dynamic compressive failure of a glass ceramic under lateral confinement. *J. Mech. Phys. Solids,* **45**, 1303-1328.

Chen, W., Zhang, B., and Forrestal, M.J. (1999). A split Hopkinson bar technique for low-impedance materials. *Exp. Mech*., **39**, 81-85.

Christensen, R.J., Swanson, S.R., and Brown, W.S. (1972). Split-Hopkinson-bar tests on rock under confining pressure. *Exp. Mech*., **29**, 508-513.

Comite Euro-International du Beton – Federation Internationale del Precontrainte (1990). CEB-FIP Model Code 90. Redwood Books, Trowbridge, Wiltshire, Great Britain.

Davies, R.M. (1948). A critical study of the Hopkinson pressure bar. *Phil. Trans. R. Soc*., **A240**, 375-457.

Duffy, J., Campbell, J.D., and Hawley, R.H. (1971). On the use of a torsional split Hopkinson bar to study rate effects in 1100-0 aluminum. *J. Appl. Mech.* **37**, 83-91.

Follansbee, P.S. and Frantz, C.E. (1983). Wave propagation in the split Hopkinson pressure bar. *J. Eng. Mater. Technol*., **105**, 61-66.

Frantz, C.E., Follansbee, P.S., and Wright, W.J. (1984). New experimental techniques with the split Hopkinson pressure bar. In I. Berman and J.W. Schroeder (Eds.), *8th International Conference on High Energy Rate Fabrication*: *Pressure Vessel and Piping division* (pp. 229-236). San Antonio, TX: ASME.

Frew, D.J. (2001). *The dynamic response of brittle materials from penetration and split Hopkinson pressure bar experiments*. ERDC/GSL TR-01-6. Vicksburg, MS: U.S. Army Engineer Research and Development Center.

Frew, D.J., Forrestal, M.J., and Chen, W. (2001). A split Hopkinson bar technique to determine compressive stress-strain data for rock materials. *Exp. Mech.,* **41**, 40-46.

Frew, D.J., Forrestal, M.J., and Chen, W. (2002). Pulse shaping techniques for testing brittle materials with a split Hopkinson pressure bar. *Exp. Mech.,* **42**, 93-106.

Graff, K.F. (1975). *Wave Motion in Elastic Solids*. Ohio: Ohio State University Press.

Gray, G.T. (2000). Classic split-Hopkinson pressure bar technique. In H. Kuhn and D. Medlin (Eds.), *ASM Handbook*, Vol. 8: *Mechanical testing and evaluation* (pp 462-476). Materials Park, OH: ASM International.

Gray, G.T. and Blumenthal, W.R. (2000). Split-Hopkinson pressure bar testing of soft materials. In H. Kuhn and D. Medlin (Eds.), *ASM Handbook*, Vol. 8: *Mechanical testing and evaluation* (pp. 488-496). Materials Park, OH: ASM International.

Gray, G.T., Idar, D.J., Blumenthal, W.R., Cady, C.M., and Peterson, P.D. (1998). High- and low-strain rate compression properties of several energetic material composites as a function of strain rate and temperature. In J.M. Short and J.E. Kennedy (Eds.), *11th Detonation Symposium* (pp. 76-84). Snowmass, CO: Amperstand Publ.

Hopkinson, B. (1914). A method of measuring the pressure produced in the detonation of high explosives or by the impact of bullets. *Philos. Trans. R. Soc. London, Ser. A,* **213**, 437-456.

Jicheng, X. and Xibing, L. (1998). The dynamic loading on rock with different loading wave shapes conventional SHPB. *J. Cent. South Univ. Technol*., **5**, 57-59.

Kolsky, H. (1949). An investigation of the mechanical properties of materials at very high rates of loading. *Proc. R. Phys. Soc. London, Ser. B*, **62**, 676-700.

Kolsky, H. (1963). *Stress Waves in Solids*. New York: Dover Publications.

Lewis, J.L. and Campbell, J.D. (1972). The development and use of a torsional Hopkinson-bar apparatus. *Exp. Mech.,* **12**, 520-524.

Lindholm, U.S. (1964). Some experiments with the split Hopkinson pressure bar. *J. Mech. Phys. Solids*, **12**, 317-335.

Lok, T.S. and Zhao, P.J. (2004). Impact response of steel fiber-reinforced concrete using a split Hopkinson pressure bar. *J. Mater. Civ. Eng.,* **16**, 1, 54-59.

Lok, T.S., Zhao, P.J., and Lu, G. (2003). Using the split Hopkinson pressure bar to investigate the dynamic behavior of SFRC. *Mag. Concr. Res.*, **55**, 183-191.

Meyers, M.A. (1994). *Dynamic Behavior of Materials*. New York: Jon Wiley and Sons, Inc.

Nemat-Nasser, S., Isaacs, J.B., and Starrett, J.E. (1991). Hopkinson techniques for dynamic recovery experiments. *Proc. R. Soc. London*, Ser. A, **435**, 371-391.

Nicholas, T. (1982). Material behavior at high strain rates. In J.A. Zukas et al. (Eds.). *Impact Dynamics*, Chapter 8 (pp. 287-307). New York: John Wiley & Sons, Inc.

Ross, C.A., Thompson, P.Y., and Tedesco, J.W. (1989). Split-Hopkinson pressure-bar tests on concrete and mortar in tension and compression. *ACI Mater. J.*, **86**, 475-481.

Schmidt, M.J. and Cazacu, O. (2006). Behavior of cementitious materials for high-strain rate conditions. *J. Phys. IV France*, **134**, 1119-1124.

Song, B, Chen, W., Antoun, B.R., and Frew, D.J. (2007). Determination of early flow stress for ductile specimens at high strain rates by using a SHPB. *Exp. Mech.,* **47**, 671-679.

Tang, T., Malvern, L.E., and Jenkins, D.A. (1992). Rate effects in uniaxial dynamic compression of concrete. *J. of Eng. Mech*., **118**, 108-124.

Williams, E.W., Akers, S.A., and Reed, P.A. (2005). *Laboratory characterization of solid grade SW brick*. ERDC/GSL TR-05-16. Vicksburg, MS: U.S. Army Engineer Research and Development Center.

Wu, X.J. and Gorham, D.A. (1997). Stress equilibrium in the split Hopkinson pressure bar test. *J. Phys. IV France*, **7**, C3-91-96.

APPENDIX A

ADDITIONAL TEST DATA FOR THE CLASSICAL SHPB TESTS

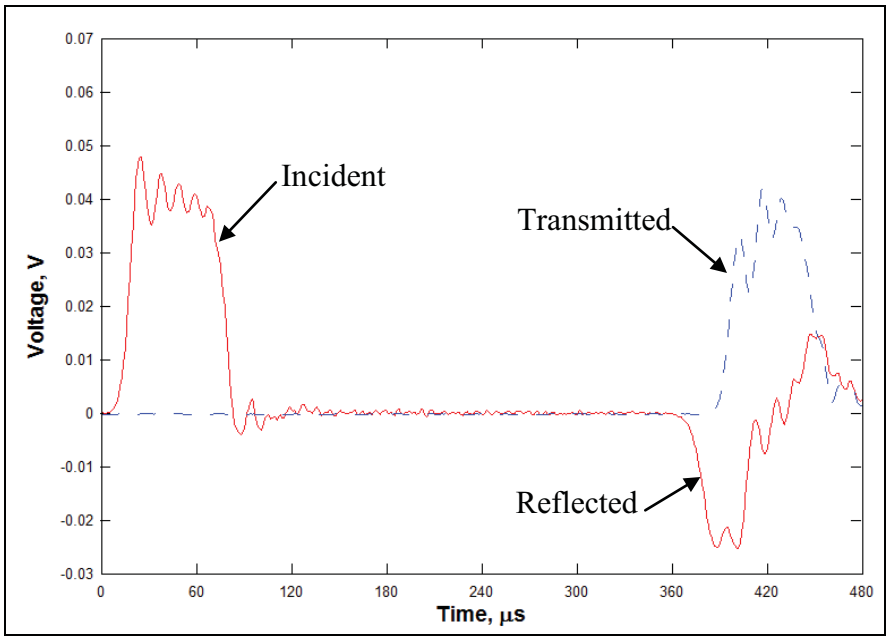

Figure 25

Voltage-Time Response from Classical SHPB Test 1A for a Brick Specimen

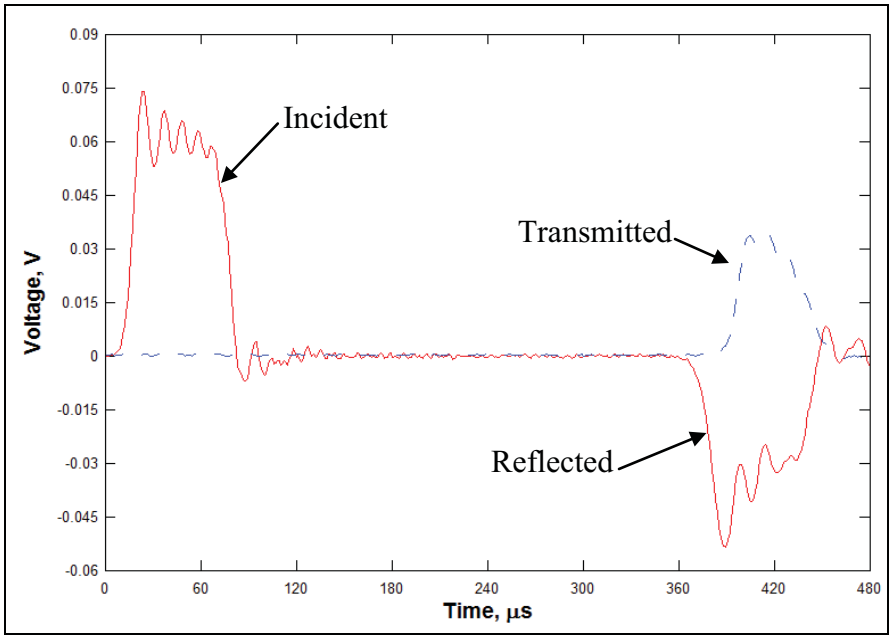

Figure 26

Voltage-Time Response from Classical SHPB Test 2A for a Brick Specimen

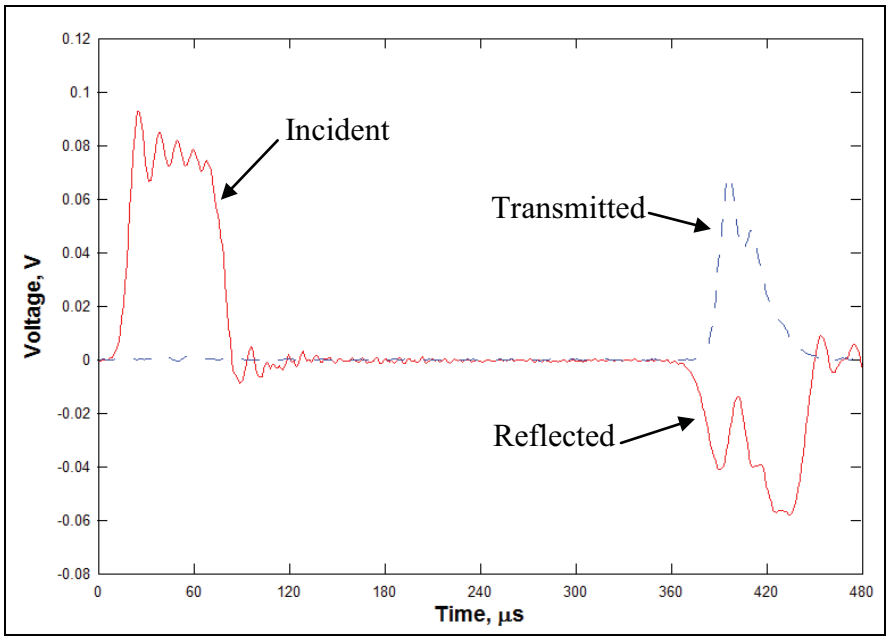

Figure 27

Voltage-Time Response from Classical SHPB Test 3A for a Brick Specimen